PHILOSOPHICAL TRANSACTIONS OF THE ROYAL SOCIETY A
MATHEMATICAL, PHYSICAL & ENGINEERING SCIENCES

Fluid Expulsion from the Cascadia Accretionary Prism: Evidence from Porosity Distribution, Direct Measurements, and GLORIA Imagery

Bobb Carson, Mark L. Holmes, Kea Umstattd, Jeffrey C. Strasser and H. Paul Johnson

Phil. Trans. R. Soc. Lond. A 1991 **335**, 331-340
doi: 10.1098/rsta.1991.0049

Fluid expulsion from the Cascadia accretionary prism: evidence from porosity distribution, direct measurements, and GLORIA imagery

By Bobb Carson[1], Mark L. Holmes[2], Kea Umstattd[3], Jeffrey C. Strasser[1] and H. Paul Johnson[4]

[1] *Department of Geological Sciences, Lehigh University, Bethlehem, Pennsylvania 18015, U.S.A.*
[2] *U.S. Geological Survey, School of Oceanography, University of Washington, Seattle, Washington 98195, U.S.A.*
[3] *Department of Geology, Carleton College, Northfield, Minnesota 55057, U.S.A.*
[4] *School of Oceanography, University of Washington, Seattle, Washington 98195, U.S.A.*

[Plate 1]

Fluid expulsion from the Cascadia accretionary prism off Oregon results from porosity reduction by compaction, and by cementation as methane-rich pore waters precipitate diagenetic carbonate deposits near the sediment-water interface. Porosity changes suggest that dewatering begins 5–6 km west of the base of the slope, in a proto-deformation zone. GLORIA imagery of surficial carbonate deposits confirms that fluid is actively expelled from this zone; there is no such evidence further west in Cascadia Basin. Within the uncertainties of the data, porosities do not decrease landward beneath the prism. This pattern is consistent with imbricate thrust faulting on the slope which provides the vertical load to induce compactive dewatering, and may physically import as much as 50% of the total fluid volume in the section. A simple vertical compaction model suggests that significant pore water volumes have been expelled from the lower slope, but at flux rates (10^{-11}–10^{-12} m^3 m^{-2} s^{-1}) which are orders of magnitude less than those measured at individual vent sites (10^{-6} m^3 m^{-2} s^{-1}). Faulting clearly controls some fluid expulsion, but GLORIA data suggest that repeated local discharge, cementation, and abandonment lead to dispersed accumulations of diagenetic carbonate.

1. Introduction

Fluid venting associated with subduction-induced sediment accretion occurs at numerous sites across the post-Oligocene portion of the Cascadia prism (Kulm & Suess 1990). Individual vents near the toe of the prism are of particular interest because they occur within a decipherable structural setting which suggests fluid transport paths. These paths may follow depositional unconformities (Lewis & Cochrane 1990), bedding, or fault zones (Moore *et al.* 1990). However, submersible and seismic reflection surveys conducted to date provide little information on the areal distribution of fluid discharge or the porosity distribution within the prism. This paper presents results from analysis of side-scan sonar (GLORIA) images and

Phil. Trans. R. Soc. Lond. A (1991) **335**, 331–340
Printed in Great Britain

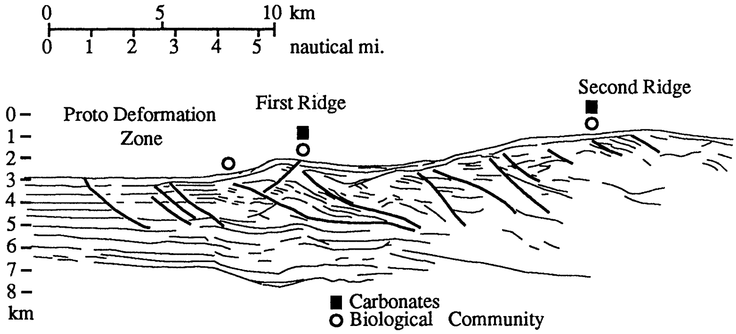

Figure 1. Interpreted depth section (after Snavely & Miller 1986) of the outer continental margin and Cascadia Basin off central Oregon. Boxes indicate approximate positions of carbonate deposits identified from submersible; circles indicate biological communities (after Moore *et al.* 1990). Faults are indicated by heavy lines.

relates them to seismic reflection and refraction data and fluid discharge measurements. The combined data-set constrains estimates of the magnitude and distribution of fluid flux on the Oregon margin.

The Oregon lower continental slope at 44° 40′ N originates as a seaward-verging, Late Pleistocene, ramp anticline (figure 1) which forms the lowermost (first) slope ridge. The frontal ramp joins the main decollement at a depth of *ca.* 2.2 km. West of the first ridge, a series of incipient thrusts that strike subparallel to the base of the slope define a proto-deformation zone, which extends 5–6 km into the Cascadia Basin. East of the first ridge is a slope basin filled with 0.5 km of Late Pleistocene sediments lying unconformably upon the thrust sheet. The second topographic ridge appears to be composed of several, older (Pleistocene–Pliocene) imbricate thrust sheets, but coherent reflections are sparse.

2. Evidence of fluid expulsion

(*a*) *Direct measurements*

Fluid expulsion has been measured at three sites on the Oregon margin (1428, 1900, and 2277, figure 2*a*). On the first ridge, flows of $1\text{–}6\times10^{-6}\ \mathrm{m^3\ m^{-2}\ s^{-1}}$ are characteristic of small vents (9–16 $\mathrm{m^2}$; Carson *et al.* 1990). At site 2277 vigorous expulsion, marked by discharge of methane bubbles and preliminary estimates of flow 3–5 times greater than those measured on the first ridge (E. Suess, personal communication), is recorded near the surface trace of a thrust fault, and apparently involves substantially larger discharge zones.

(*b*) *Porosity reduction*

Porosity distributions for the Cascadia margin (figure 3) are derived from compressional wave velocities determined by seismic refraction (Lewis 1990), and from migration analysis of multichannel reflection lines which corroborate the refraction data (Cochrane *et al.* 1990). Higher velocities beneath the first ridge of the lower slope were derived by Klaeschen & von Huene (1990), but are not used here. Refraction results (Cochrane *et al.* 1988) are utilized beneath the second ridge as poor reflector coherence precludes reliable migration analysis. The derived porosity distribution beneath the second ridge must be considered tentative.

PHILOSOPHICAL TRANSACTIONS OF THE ROYAL SOCIETY A MATHEMATICAL, PHYSICAL & ENGINEERING SCIENCES

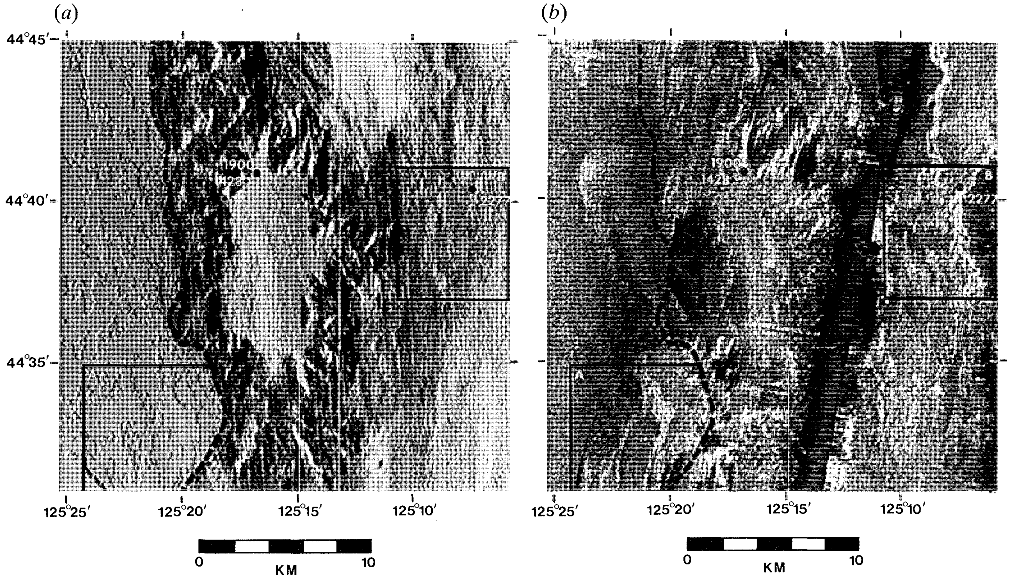

Figure 2. (*a*) Derivative map of SeaBeam bathymetry showing bottom slope of the lower margin and Cascadia Basin off Oregon. Subareas (A) and (B) exhibit minor variations in bottom slope. (*b*) GLORIA image of same areas as figure 2*b*. Base of the continental slope is indicated by the dashed line. Sites 1428, 1900, and 2277 are *Alvin* dive sites at which carbonates were sampled. GLORIA trackline (zone of no data) extends from 125° 10′ W at top of image to 125° 14′ W at the bottom. East of this track the bottom is insonified from the west. West of the track, the near bottom is insonified from the east. Cascadia Basin, on the far left side of the figure has been insonified from the west as part of the adjacent swath. The join between the two swaths can be seen at 125° 17′ W (top); it proceeds irregularly to 124° 24′ W (bottom).

The velocity–porosity conversion is based on more than 600 data points derived from well logs on the Washington margin, from shipboard logs of Deep Sea Drilling Program (DSDP) sites 174 and 175, and from analysis of returned samples (Strasser 1989). Regression on the velocity–porosity data is mediocre ($r = 0.82$), because carbonate cementation (see below) modifies the rigidity modulus as well as density in the compressional wave velocity equation (Lewis 1990). Although we suspect that carbonate cementation is relatively minor below several metres sub-bottom (based on carbonate occurrence at DSDP sites 174 and 175), any cementation would increase the seismic velocity and reduce the derived porosity in a way that differs from simple compactive change. Nevertheless, those effects are incorporated in our regression equation. The velocity–porosity relationship used here probably underestimates the actual porosity, as indicated by the low values calculated for Cascadia Basin deposits compared with measured porosities from DSDP site 174 (figure 3). However, the absolute values of porosity are of secondary importance because we are interested here in relative changes in porosity across the lower prism.

Porosities on the Oregon margin are apparently lower than porosities in distal portions (greater than 20 km west of margin toe) of Cascadia Basin (figure 3). The porosity loss across the deformation front, which averages about 4% to a depth of 2.0 km, has been attributed to compaction associated with accretion (Carson 1977; Davis *et al.* 1990), and to exposure of previously buried section (Cochrane *et al.* 1988).

However, the regional landward reduction in sediment porosity inferred for many accretionary prisms (Bray & Karig 1985) is not apparent at the toe of the Oregon

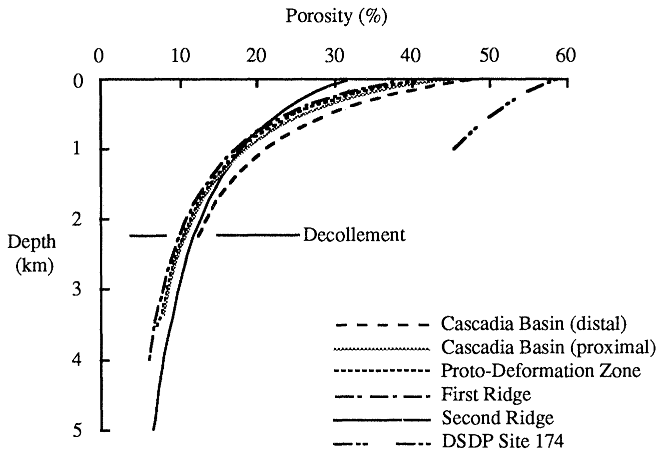

Figure 3. Porosity–depth profiles for Cascadia Basin and lower slope, based on seismic refraction results (first ridge, Lewis 1990; second ridge, Cochrane *et al.* 1988), interval migration velocities (Cascadia basin and proto-deformation zone, Cochrane *et al.* 1990), and the velocity–porosity distribution for the Cascadia margin (Strasser 1989). Porosity (n)–depth (m) regression lines are: (1) distal Cascadia Basin: $1/n = 2.14528+2.71205\text{E-}3(\text{m})$, $r = 0.94$, 19 d.f.; (2) proximal Cascadia Basin: $1/n = 2.31979+3.15217\text{E-}3(\text{m})$, $r = 0.92$, 27 d.f.; (3) proto-deformation zone: $1/n = 2.48078+3.20834\text{E-}3(\text{m})$, $r = 0.93$, 34 d.f.; (4) first ridge: $1/n = 2.46752+3.41516\text{E-}3(\text{m})$, $r = 0.99$, 26 d.f.; (5) second ridge: $1/n = 3.31991+2.29109\text{E-}3(\text{m})$, $r = 0.99$, 4 d.f.; (6) DSDP site 174: $1/n = 1.75218+4.57154\text{E-}4(\text{m})$, $r = 0.53$, 15 d.f.

slope (Strasser *et al.* 1989; Lewis 1990). Porosities in the proto-deformation zone, and the first ridge are indistinguishable, and beneath the second ridge are not significantly different (figure 3). The porosity distributions superficially suggest significant fluid expulsion from the proto-deformation zone, but fluid retention beneath the first ridge, and perhaps the second, since no systematic landward decrease in porosity is apparent.

(*c*) *Diagenetic carbonate deposition*

Where fluid discharge occurs on Cascadia and other convergent margins, authigenic carbonate deposits are formed by oxidation of dissolved methane (Kulm *et al.* 1986; Kastner *et al.* 1987; Le Pichon *et al.* 1987; Ritger *et al.* 1987; Kulm & Suess 1990). On the Cascadia margin some carbonates are exposed at the seafloor, but much of the carbonate deposition takes place by anaerobic methane oxidation within the sulphate-reducing zone (i.e. the upper 2–10 m; Suess & Massoth 1984) of the sediment column (Ritger *et al.* 1987; Han & Suess 1987). As these near-surface carbonates are positive indicators of pore fluid discharge, their extent and position on the accretionary prism are a record of the magnitude and structural/stratigraphic control of past expulsion.

Because carbonates have a significantly greater acoustic impedance ($9\text{–}12\times10^6$ kg m^{-2} s^{-1}) than unconsolidated sediment (2×10^6 kg m^{-2} s^{-1}; Johnson & Helferty 1990), the diagenetic carbonate deposits can be imaged by side-scan sonar at the seafloor (reflection coefficient is 0.71–0.77) and beneath a veneer of mud, as the reflection coefficient across the water–mud interface is only 0.13, but from unconsolidated mud to carbonates is 0.64–0.71. Other factors affect the amplitude of GLORIA backscatter, but in areas where the slope and surface roughness are constant, carbonate deposits in unconsolidated sediments are readily detected. Consolidated

PHILOSOPHICAL TRANSACTIONS OF THE ROYAL SOCIETY A MATHEMATICAL, PHYSICAL & ENGINEERING SCIENCES

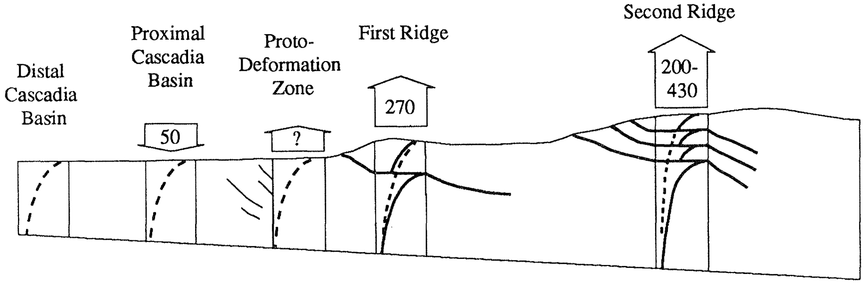

0.23		0.17		0.16		0.13	Model		0.11	Average porosity
2.1		3.2		3.4		4.3	1.5 / 2.8	4.3-4.8	6.0-6.5	Thickness (km)
480		530		530		570	840	940-1070	720-750	Porewater vol. ($m^3 m^{-2}$)
		-10		?		47			25-50	% present vol. expelled
						2.9×10^{-11} - 4.3×10^{11}			1.1×10^{-11} - 3.0×10^{-12}	Apparent rate of expul. ($m^3 m^{-2} s^{-1}$)

Figure 4. Schematic diagram of porosity, fluid inventory, and expulsion volumes for the Cascadia margin. Conceptual porosity–depth profiles associated with instantaneous thrust-faulting are shown by heavy lines; representations of observed profiles (figure 3) indicated by dashed lines. Calculated expulsion (or incorporation) volumes are shown in arrows, which imply nothing about mode of discharge. Pore fluid volumes for each location are tabulated beneath the diagram. See text for explanation of computations.

sandstones and shales are also strong reflectors (acoustic impedance is 7×10^6 kg m^{-2} s^{-1}; seafloor reflectance coefficient is 0.64) and occur in this area (Kulm *et al*. 1986). Although carbonates are superior reflectors relative to sandstones and shales, the acoustic impedance contrast (12.5%) is not sufficiently large that they can be reliably differentiated; identification must be made on the basis of geometry or independent (submersible) observation.

Sites of significant carbonate deposition (1900, 2277; figure 2*b*) observed from the submersible *Alvin* appear as regions of very strong backscatter in GLORIA imagery. Not all carbonate deposition is imaged, however; where carbonate precipitation is areally restricted (e.g. 1428, 9 m^2 as mapped from *Alvin*; figure 2*b*) or zones where precipitation occurs at subsurface depths greater than those penetrated by the acoustic signal (greater than 0.5–2 m) are not defined in the GLORIA images. Interpretation is complicated by the fact that bottom topography affects the angle of insonification, and high-amplitude backscatter (identical to returns from carbonate deposits) is produced at high reflectance angles. Nevertheless, we can assess the areal distribution of carbonate deposition in those regions where the bottom slope remains relatively constant (A, B; figure 2).

3. Fluid expulsion on the Oregon accretionary prism

(*a*) *Cascadia Basin*

Although average porosity decreases in Cascadia Basin from west to east, pore water volume increases as deposition thickens the sediment column (figure 4). At any given depth, however, the carbonate is lower near the margin (figure 3) which may

PHILOSOPHICAL TRANSACTIONS OF THE ROYAL SOCIETY A MATHEMATICAL, PHYSICAL & ENGINEERING SCIENCES

indicate lateral textural variations or that the effects of tectonic stress extend seaward of the proto-deformation zone. The GLORIA data show no evidence of near-surface carbonate deposition in Cascadia Basin at distances of greater than 6 km west of the base of the continental slope.

(b) *Proto-deformation zone*

Blind thrusts extend to at least 2.2 km depth (figure 1) and show reversed polarity on multichannel seismic lines, suggesting higher, local porosity. If so, they may be active fluid conduits (J. C. Moore, personal communication). If the faults have delivered a significant fluid volume to the surface, the effect of that dewatering should be apparent in both the porosity and GLORIA data.

Porosity is lower at all comparable depths in the proto-deformation zone than in Cascadia Basin (figure 3). Integration and comparison of the porosity–depth profiles from proximal Cascadia Basin and the proto-deformation zone indicates indistinguishable pore fluid volumes, although the sediment section has thickened by 200 m (figure 4). Thickening results from some combination of deposition and small-displacement thrust faulting. The porosity data are insufficiently precise to indicate whether or not fluids are expelled in this region.

Although GLORIA imagery does not indicate strong backscattering uniformly across the proto-deformation zone, clear evidence of cementation is apparent between 44° 31′ N and 44° 35′ N (figures 2*b*, 5, plate 1). Flat-lying Cascadia Basin deposits (figure 2*a*) show high-amplitude backscatter in an anastamosing pattern which evolves into a slope-parallel fault trace to the south (44° 28′ N to 44° 12′ N). The geometry and backscattering levels preclude a clastic deposit and there is no apparent correlation with topography. Diffuse areas of strong reflectance to the north (44° 41′ N and 44° 44′ N, figure 2*b*) are more problematic; they may indicate carbonate deposition or small, sand-rich fan deposits.

(c) *First ridge*

Although porosity–depth distributions for the proto-deformation zone and first ridge are virtually identical (figure 3), the fluid budget is complicated by tectonic thickening (thrust-faulting). The ridge was built by imbricate thrusting of pre-existing proto-deformation deposits over proximal Cascadia Basin sediments. A conceptual model (figure 4, First Ridge; Strasser 1989) assumes instantaneous faulting of a 1500 m proto-deformation section over 2800 m of Cascadia Basin sediments. This tectonic movement substantially increases the pore fluid volume beneath the ridge (to 840 $m^3\ m^{-2}$; the analysis is quite insensitive to the position of the fault), and with burial of the highly porous lower section, induces porosity reduction by vertical compaction. A rough estimate of the fluid discharged, obtained by subtracting the present fluid volume (570 $m^3\ m^{-2}$) from the calculated, tectonically emplaced volume, is 270 $m^3\ m^{-2}$; 47% of the present fluid volume. The analysis clearly suggests substantial fluid loss.

GLORIA data across the first ridge and associated slope basin are difficult to interpret. Although very strong backscattering is observed at *Alvin* site 1900 (figure 2*b*), and around the perimeter of the slope basin, most of the highest-amplitude reflectance appears to be topographically controlled. The ridge is characterized by low reflectance along its crest and seaward flank. The slope basin exhibits generally strong backscattering that might reflect widespread, diffusive discharge and cementation. Even this pattern has a topographic component, however; the highest

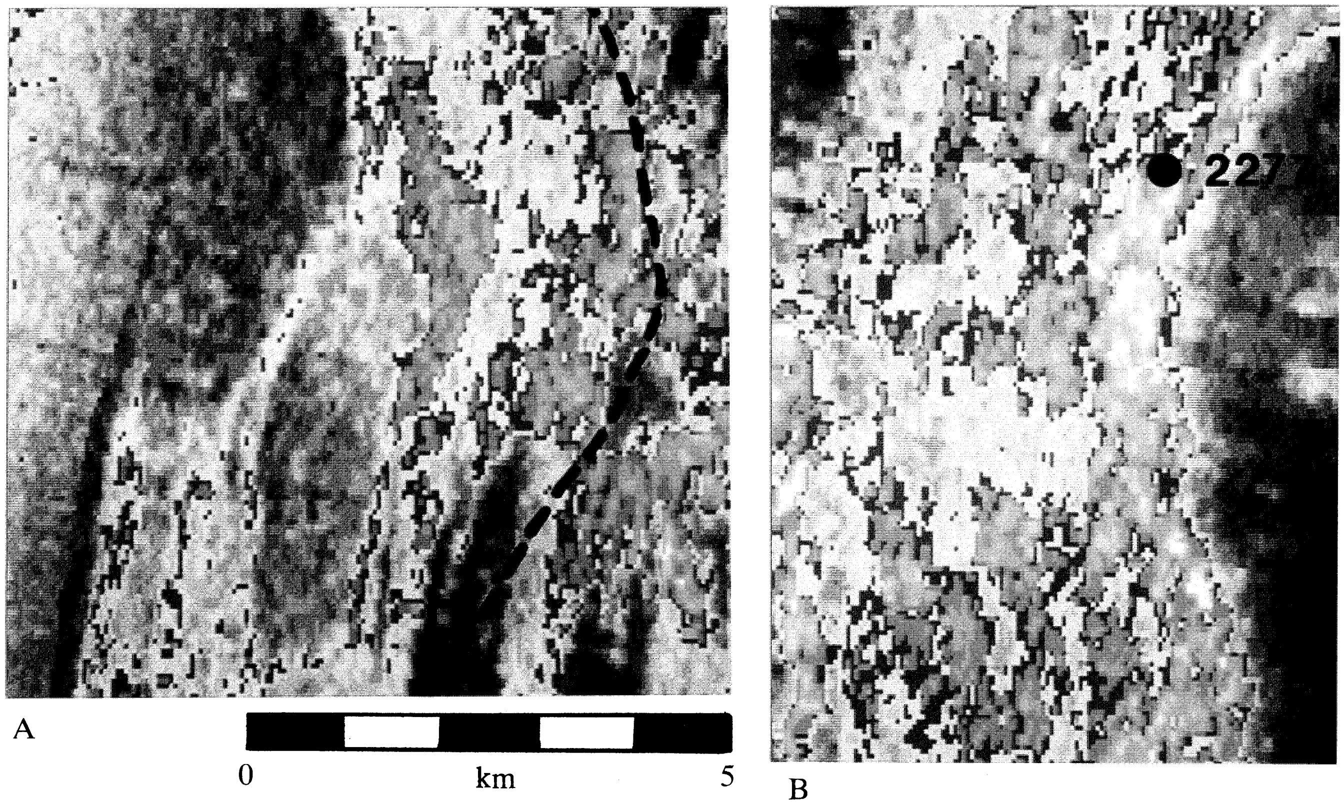

Figure 5. Enlargements of GLORIA imagery in subareas (A) and (B), figure 2*b*. Coloured areas comprise pixels in the upper 37% of the reflectance spectrum. Lower levels of backscattering are rendered in grey. Within the coloured zones, reflectance increases from purple to light yellow. Strongest reflectors lie south and northeast of *Alvin* site 2277, in the middle of a band of very strong backscattering. Dashed line in (A) is the base of the continental slope (figure 2*a*).

PHILOSOPHICAL TRANSACTIONS OF THE ROYAL SOCIETY A MATHEMATICAL, PHYSICAL & ENGINEERING SCIENCES

amplitudes are associated with the broad upwarping of the western half of the basin. Submersible surveys in the slope basin reveal no evidence of carbonate deposition.

If the first ridge was elevated between 200000 and 300000 years before present (BP) (Kulm & Fowler 1974), the calculated discharge volume (figure 4) would have been expelled at rates of $2.9–4.3 \times 10^{-11}\ m^3\ m^{-2}\ s^{-1}$. These values are five orders of magnitude less than measured venting rates at sites 1428 and 1900 (Carson *et al.* 1990).

(*d*) *Second ridge*

Cementation on the second ridge is extensive (figure 2*b*, 5) but areally variable. Very strong reflectance in the GLORIA imagery occurs at site 2277, where large (greater than $3 \times 10^4\ m^2$), surficial carbonate deposits were observed in several *Alvin* dives (J. C. Moore, personal communication). This site is associated with a fault (figure 1) that supports vigorous discharge. The GLORIA data, however, indicate that cementation is not restricted to this particular locality; strong backscattering characterizes the western flank of the ridge between 44° 37′ N and 44° 41′ N, at depths ranging from 1300–700 m. The reflectance pattern defines two particular zones that could be construed as fault traces: one is the very strong backscattering associated with site 2277; the other is a band of high reflectance which trends nearly north–south at 125° 8.5′ W, between 44° 41.5′ N and 44° 45.5′ N (figures 2*b*, 5). The latter follows a zone of increased bottom slope (figure 2*a*), but the strength of backscattering is out of proportion to the change in slope, and we infer that cementation and fluid expulsion have occurred here. The remainder of the slope (figure 5) is characterized by intermediate to high backscattering which occurs in a complex, distributed pattern that suggests almost random point discharges and cementation. Perhaps the pattern results from long-standing dewatering in which individual expulsion sites are activated and then abandoned with some regularity.

The porosity beneath the second ridge decreases from an anomalously low 32% at the surface (which may reflect the extensive cementation) to about 8% at a depth of 4 km (figure 3). The conceptual model of near-surface thrust-faulting to thicken the section (figure 4) assumes repetition of this porosity–depth relationship. Thickening due to faulting at depths greater than 2 km has an insignificant effect (less than $20\ m^3\ m^{-2}$) on the calculated fluid inventory. However, the fluid volume is fairly sensitive to the number of imbricate thrust packets emplaced near the surface, and to the total thickness of the section. The variation in predicted porewater volume ($940–1070\ m^3\ m^{-2}$; figure 4) reflects emplacement of one versus three thrust packets over the same vertical extent (1700 m). Comparing these predicted volumes with the present estimated porewater volume ($720–750\ m^3\ m^{-2}$) suggests expulsion of $190–350\ m^3\ m^{-2}$, or about 25–50% of the present fluid inventory. This is a maximum estimate as the model assumes that thickening has occurred exclusively near the surface. The extensive carbonate deposition observed from *Alvin* at site 2277 and the GLORIA data both indicate an extensive expulsion history.

Radiolarian biostratigraphy suggests that the second ridge was uplifted $1–2 \times 10^6$ years ago (L. D. Kulm, personal communication). If expulsion of the estimated $190–350\ m^3\ m^{-2}$ occurred over that period, average fluid discharge rates have been $1.1 \times 10^{-11}–3.0 \times 10^{-12}\ m^3\ m^{-2}\ s^{-1}$. As on the first ridge, these rates are orders of magnitude less than flow rates measured at vent site 2277 (E. Suess, personal communication).

4. Implications for fluid expulsion

GLORIA data confirm that fluids are delivered to the sediment–water interface in the proto-deformation zone (figure 5). Carbonate deposition clearly takes place at or near the sediment surface, but initially it may also occur in the shallow subsurface (less than 200 MBSF) as advecting methane-saturated fluids are anaerobically oxidized by sulphate reduction (Ritger *et al.* 1987; Han & Suess 1989). Because cementation inevitably leads to porosity reduction and decreased permeability near the top of the sediment column, continued flow is probably accommodated by repeated faulting and development of a fracture permeability (J. C. Moore *et al.*, this symposium). We suggest that this process and significant surface expulsion begin in the proto-deformation zone.

Surficial dewatering in the proto-deformation zone is terminated by overthrusting associated with advance of the prism toe. The advance presumably buries the surface and near-surface carbonates deposited in the proto-deformation zone and incorporates them in the tectonic stack, where they may be preserved or undergo dissolution and redistribution. Excess pore pressure is generated beneath the thrust sheet (Wang *et al.* 1990), perhaps driving flow upward through the hanging wall along pre-existing proto-thrust faults or new fractures developed during thrusting. Burial of cold, porous, near-surface sediments beneath the advancing thrust sheet creates a high-porosity reservoir, dominated by low-temperature fluids (Shi *et al.* 1988). To date, all fluids recovered from this area exhibit biogenic methane (E. Suess, personal communication), which implies burial temperatures less than 75 °C (Ritger *et al.* 1987).

Fluid expulsion on the first ridge is probably largely controlled by faulting (Moore *et al.* 1990), although diapiric structures may be locally important (Lewis & Cochrane 1990). By the time the ridge is elevated, advection has displaced the sulphate reducing zone to the surface (Han & Suess 1988) and dictates that cementation is almost wholly a surficial (less than 2–10 MBSF) phenomenon. Vent sites supported by fractures are frequently initiated and abandoned as cementation reduces surface permeability. Nevertheless, discharge is a local phenomenon; there is no obvious side-scan sonar evidence to support widespread expulsion and cementation.

The second ridge is characterized by extensive cementation. The greatest concentrations occur in two, well-defined zones that parallel the strike of the regional slope. One of these (Site 2277, figure 2*b*) is the surface trace of a thrust fault. Other strong backscattering on the second ridge is dispersed, however, and does not suggest fault control. It is not clear whether the complex cementation pattern (north as well as south and west of site 2277, figure 5) represents relict fault control complicated by post-depositional dissolution, or whether active venting is inhomogeneously dispersed across the slope. Davis *et al.* (1990) suggest areally pervasive vertical flow for the northern Cascadia margin. If the extensive backscattering on the second ridge indicates dispersed vertical flow, it is a marked departure from the character of discharge further seaward off Oregon, and may indicate development of a different dispersal mechanism, such as extensive small-scale fracturing.

Although uncertainties in the velocity–porosity relationship and in the importance of horizontal advection limit the usefulness of the thrust-sheet loading/vertical compaction model, it provides some insights. Clearly horizontal fluid transport by thrust sheet emplacement is an important component of the fluid budget. Not only does the thrust sheet provide the vertical load to induce compactive dewatering, but

PHILOSOPHICAL TRANSACTIONS OF THE ROYAL SOCIETY A MATHEMATICAL, PHYSICAL & ENGINEERING SCIENCES

it may physically import as much as 50% of the total fluid volume in the section. Although the calculated discharge rates (10^{-11}–10^{-12} m^3 m^{-2} s^{-1}, figure 4) are suspect, they provide gross estimates of the flux that is supportable by compaction alone. Regardless of the error inherent in those estimates, they cannot be reconciled with measured rates of venting ($1–6 \times 10^{-6}$ m^3 m^{-2} s^{-1}; Carson *et al.* 1990).

The GLORIA data, which suggest that significant cementation associated with expulsion covers a relatively small portion of the margin, dictate that the disparity between the estimated rates of outflow derived from porosity change and measured expulsion rates at vents requires both channelling of flow by high permeability zones and non-steady-state discharge. Beyond this point, the problem is underconstrained; we need to determine the duration and magnitude of site-specific venting if we are to determine the volume of the fluid reservoir that supports it. Dating the carbonate deposits and geochemically relating their volume to the volume of depositing fluids would be an important contribution to resolving the fluid budget.

This work was funded by grants from the National Science Foundation (OCE-8613501) and JOI/U.S. Science Support Program (JSC-8-90). B. T. R. Lewis and G. Cochrane conducted the refraction survey and provided velocity analysis. G. Cochrane and R. von Huene generously shared velocity results from their MCS migration analyses. D. Twitchell and V. Paskevich provided invaluable assistance in processing the GLORIA and SeaBeam data. The typescript benefited significantly from reviews by J. C. Moore and an anonymous referee.

References

Bray, C. J. & Karig, D. E. 1985 Porosity of sediments in accretionary prisms, and some implications for dewatering processes. *J. geophys. Res.* **90**, 768–778.

Carson, B. 1977 Tectonically-induced deformation of deep-sea sediments off Washington and Oregon: mechanical consolidation. *Mar. Geol.* **24**, 289–307.

Carson, B., Suess, E. & Strasser, J. C. 1990 Fluid flow and mass flux determinations at vent sites on the Cascadia margin accretionary prism. *J. geophys. Res.* **95**, 8891–8897.

Cochrane, G. R., Lewis, B. T. R. & McClain, K. J. 1988 Structure and subduction processes along the Oregon–Washington margin. *Pure appl. Geophys.* **128**, 767–800.

Cochrane, G. R., Moore, J. C., Mackay, M. & Moore, G. F. 1990 Fluid flow in the Oregon accretionary prism from seismic data and vents. *Eos, Wash.* **71**, 1580.

Davis, E. E., Hyndman, R. D. & Villinger, H. 1990 Rates of fluid expulsion across the northern Cascadia accretionary prism: constraints from new heat flow and multichannel seismic reflection data. *J. geophys. Res.* **95**, 8869–8889.

Han, M. W. & Suess, E. 1989 Subduction-induced pore fluid venting and the formation of authigenic carbonates along the Oregon/Washington continental margin: implications for the global Ca cycle. *Paleogeogr. Paleoclimat. Paleoecol.* **71**, 119–136.

Johnson, H. P. & Helferty, M. 1990 The geological interpretation of side-scan sonar. II. Processing and analysis of images. *Rev. Geophys.* **28**, 357–380.

Kastner, M., Suess, E., Garrison, R. E. & Kvenvolden, K. 1987 Hydrology, geochemistry, and diagenesis along the convergent margin off Peru. *Eos, Wash.* **68**, 1499.

Klaeschen, D. & von Huene, R. 1990 Ocean Drilling Program site survey seismic record – Oregon. *Fluids in Accretionary Prisms* (abstr.), Paris.

Kulm, L. D. & Fowler, G. A. 1974 Oregon continental margin structure and stratigraphy: a test of the imbricate thrust model. In *The geology of continental margins* (ed. C. A. Burke & C. L. Drake), pp. 261–284. New York: Springer-Verlag.

Kulm, L. D., Suess, E., Moore, J. C., Carson, B., Lewis, B. T., Ritger, S., Kadko, D., Thornburg, T., Embley, R., Rugh, W., Massoth, G. J., Langseth, M., Cochrane, G. R. & Scamman, R. L. 1986 Oregon subduction zone: Venting, fauna, and carbonates. *Science, Wash.* **231**, 561–566.

Kulm, L. D. & Suess, E. 1990 Relationship between carbonate deposits and fluid venting: Oregon accretionary prism. *J. geophys. Res.* **95**, 8899–8915.

Le Pichon, X. *et al.* 1987 Nankai Trough and Zenisu Ridge: a deep-sea submersible survey. *Earth planet. Sci. Lett.* **83**, 285–299.

Lewis, B. T. R. 1990 Changes in P and S velocities caused by subduction related sediment accretion off Washington/Oregon, NATO Conference on Shear Waves in Marine Sediments. (Submitted.)

Lewis, B. T. R. & Cochrane, G. R. 1990 Relationship between the location of chemosynthetic benthic communities and geologic structure on the Cascadia subduction zone. *J. geophys. Res.* **95**, 8783–8794.

Moore, J. C., Orange, D. & Kulm, L. D. 1990 Interrelationship of fluid venting and structural evolution: *Alvin* Observations from the frontal accretionary prism, Oregon. *J. geophys. Res.* **95**, 8795–8808.

Ritger, S., Carson, B. & Suess, E. 1987 Methane-derived authigenic carbonates formed by subduction-induced pore water expulsion along the Oregon/Washington margin. *Geol. Soc. Am. Bull.* **98**, 147–156.

Shi, Y., Wang, C., Langseth, M. G., Hobart, M. & von Huene, R. 1988 Heat flow and thermal structures of the Washington/Oregon accretionary prism – a study of the lower slope. *Geophys. Res. Lett.* **15**, 1113–1116.

Snavely, P. D., Jr & Miller, J. 1986 The central Oregon continental margin, lines WO76-4 and WO76-5. In *Seismic images of modern convergent margin tectonic structure* (ed. R. von Huene). *AAPG Stud. Geol.* **26**, 24–29.

Strasser, J. C. 1989 Velocity-derived porosity distribution of the Oregon margin: implications for sediment dewater at the toe of the accretionary prism. M.S. thesis, Lehigh University, Department of Geological Sciences, Bethlehem, Pennsylvania.

Strasser, J. C., Carson, B. & Lewis, B. T. R. 1989 Velocity-derived porosity distribution of the lower Oregon margin accretionary prism: implications for dewatering. *Geol. Soc. Am., Abstr. Progr.* A **21**, 312.

Suess, E. & Massoth, G. J. 1984 Evidence for venting of pore waters from subducted sediments of the Oregon continental margin. *Eos, Wash.* **65**, 1089.

Wang, C.-Y., Shi, Y., Hwang, W.-T. & Chen, H. 1990 Hydrogeologic processes in the Oregon–Washington accretionary complex. *J. geophys. Res.* **95**, 9009–9023.

Colour plate printed in Great Britain by George Over Limited, London and Rugby

PHILOSOPHICAL TRANSACTIONS OF THE ROYAL SOCIETY A MATHEMATICAL, PHYSICAL & ENGINEERING SCIENCES

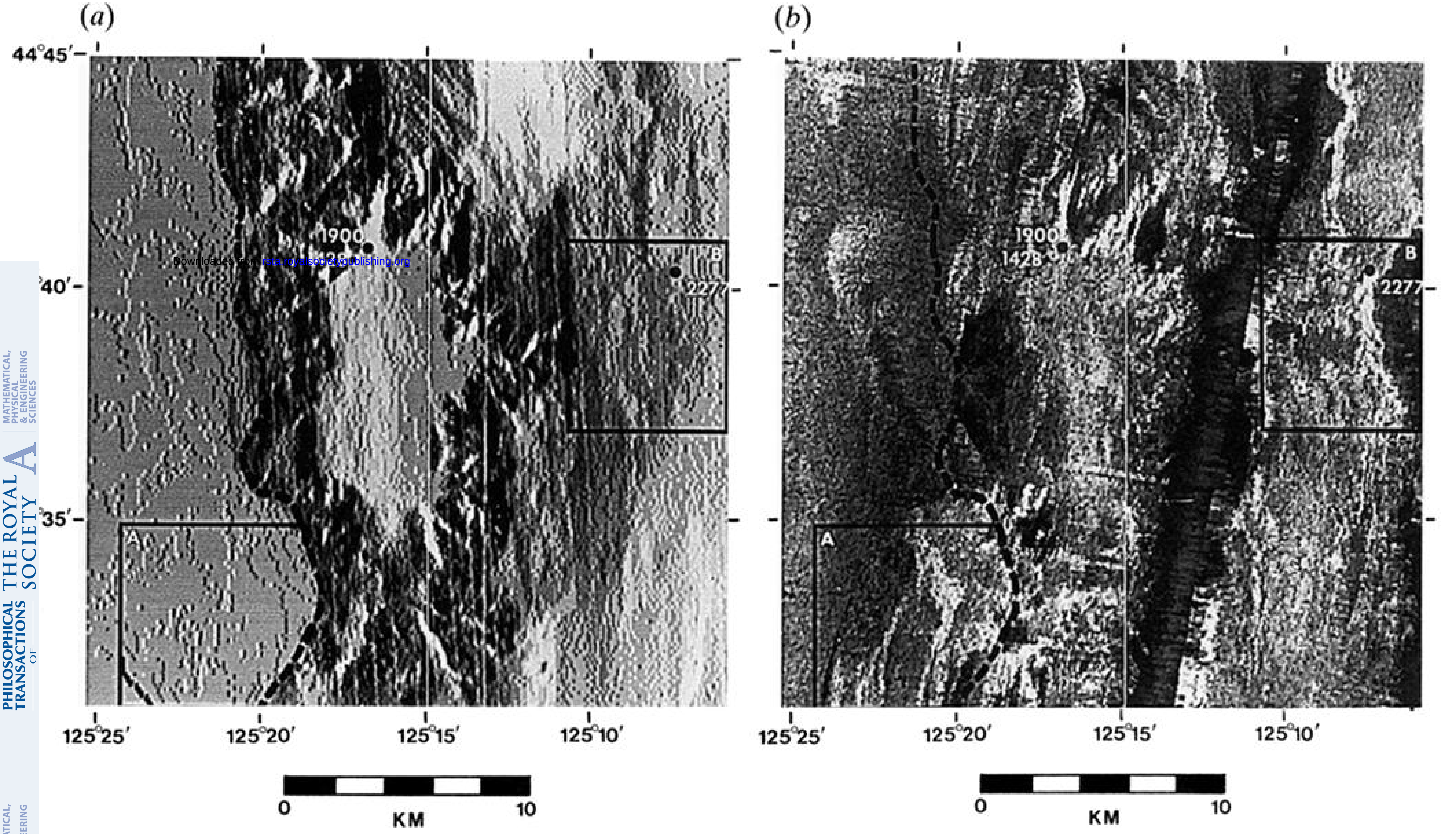

igure 2. (*a*) Derivative map of SeaBeam bathymetry showing bottom slope of the lower margin nd Cascadia Basin off Oregon. Subareas (A) and (B) exhibit minor variations in bottom slope. (*b*) LORIA image of same areas as figure 2*b*. Base of the continental slope is indicated by the dashed ne. Sites 1428, 1900, and 2277 are *Alvin* dive sites at which carbonates were sampled. GLORIA rackline (zone of no data) extends from 125° 10′ W at top of image to 125° 14′ W at the bottom. ast of this track the bottom is insonified from the west. West of the track, the near bottom is nsonified from the east. Cascadia Basin, on the far left side of the figure has been insonified from he west as part of the adjacent swath. The join between the two swaths can be seen at 125° 17′ W op); it proceeds irregularly to 124° 24′ W (bottom).

PHILOSOPHICAL TRANSACTIONS OF THE ROYAL SOCIETY A MATHEMATICAL, PHYSICAL & ENGINEERING SCIENCES

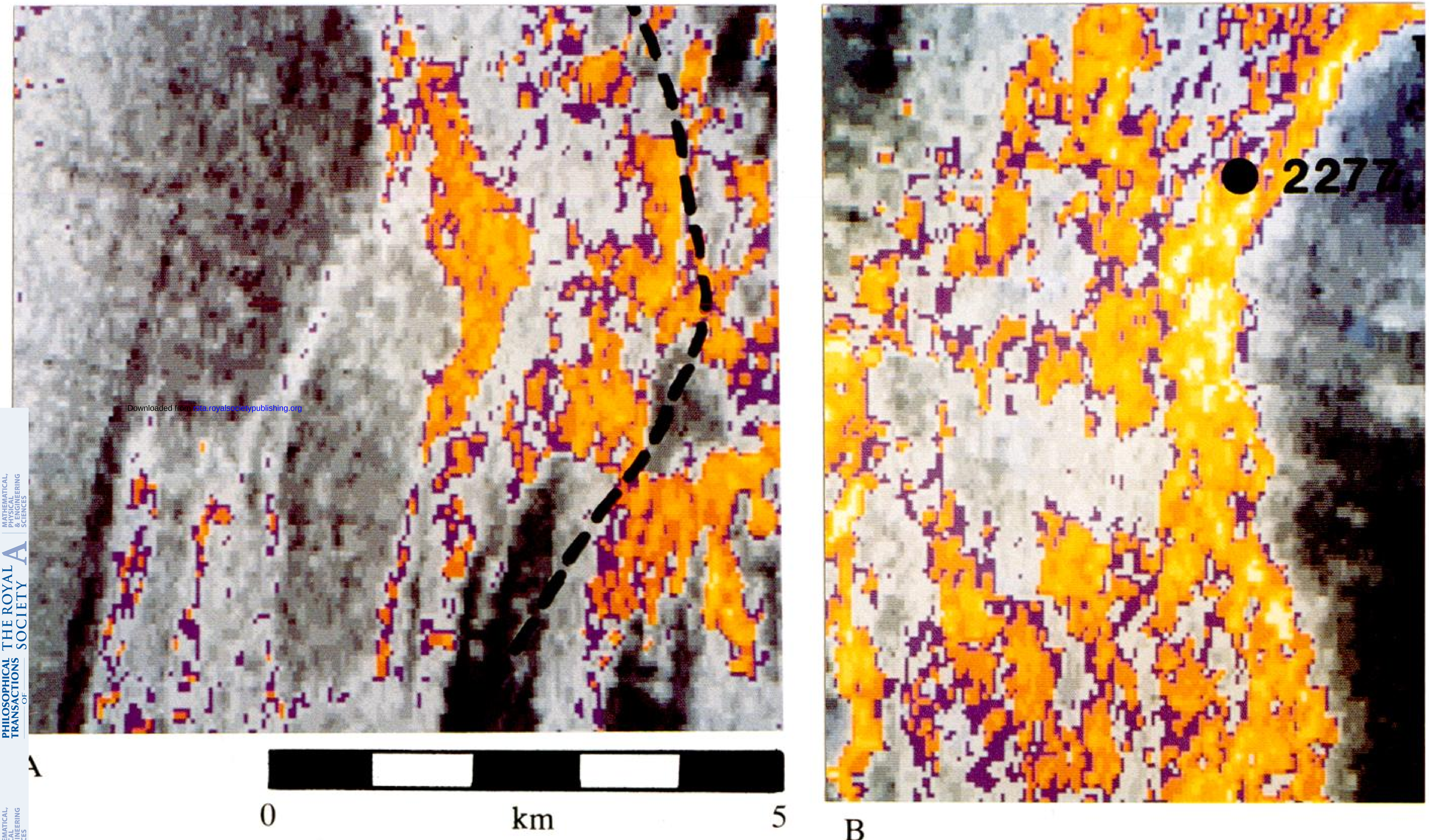

Figure 5. Enlargements of GLORIA imagery in subareas (A) and (B), figure 2*b*. Coloured areas comprise pixels in the upper 37% of the reflectance spectrum. Lower levels of backscattering are rendered in grey. Within the coloured zones, reflectance increases from purple to light yellow. Strongest reflectors lie south and northeast of *Alvin* site 2277, in the middle of a band of very strong backscattering. Dashed line in (A) is the base of the continental slope (figure 2*a*).

PHILOSOPHICAL TRANSACTIONS OF THE ROYAL SOCIETY A MATHEMATICAL, PHYSICAL & ENGINEERING SCIENCES